

# Disruption of the Sarcoglycan–Sarcospan Complex in Vascular Smooth Muscle: A Novel Mechanism for Cardiomyopathy and Muscular Dystrophy

Ramon Coral-Vazquez,<sup>1,7</sup> Ronald D. Cohn,<sup>1,7</sup> Steven A. Moore,<sup>2</sup> Joseph A. Hill,<sup>4</sup> Robert M. Weiss,<sup>4</sup> Robin L. Davisson,<sup>5</sup> Volker Straub,<sup>1</sup> Rita Barresi,<sup>1</sup> Dimple Bansal,<sup>1</sup> Ron F. Hrstka,<sup>3</sup> Roger Williamson,<sup>3</sup> and Kevin P. Campbell<sup>1,6</sup>

<sup>1</sup>Howard Hughes Medical Institute  
Department of Physiology and Biophysics  
and Department of Neurology

<sup>2</sup>Department of Pathology

<sup>3</sup>Department of Obstetrics and Gynecology  
University of Iowa College of Medicine  
Iowa City, Iowa 52242

<sup>4</sup>Department of Veterans Affairs  
Iowa City, Iowa 52242

and Department of Internal Medicine

<sup>5</sup>Department of Anatomy and Cell Biology  
University of Iowa  
Iowa City, Iowa 52242

## Summary

To investigate mechanisms in the pathogenesis of cardiomyopathy associated with mutations of the dystrophin–glycoprotein complex, we analyzed genetically engineered mice deficient for either  $\alpha$ -sarcoglycan (*Sgca*) or  $\delta$ -sarcoglycan (*Sgcd*). We found that only *Sgcd* null mice developed cardiomyopathy with focal areas of necrosis as the histological hallmark in cardiac and skeletal muscle. Absence of the sarcoglycan–sarcospan (SG-SSPN) complex in skeletal and cardiac membranes was observed in both animal models. Loss of vascular smooth muscle SG-SSPN complex was only detected in *Sgcd* null mice and associated with irregularities of the coronary vasculature. Administration of a vascular smooth muscle relaxant prevented onset of myocardial necrosis. Our data indicate that disruption of the SG-SSPN complex in vascular smooth muscle perturbs vascular function, which initiates cardiomyopathy and exacerbates muscular dystrophy.

## Introduction

Dilated cardiomyopathy is a multifactorial disease that includes both inherited and acquired forms of cardiomyopathy. Inherited cardiomyopathy in humans can be associated with genetic defects occurring in components of the dystrophin–glycoprotein complex (DGC) (Towbin, 1998). In both skeletal and cardiac muscle, the DGC consists of dystrophin, the syntrophins,  $\alpha$ - and  $\beta$ -dystroglycan ( $\alpha$ -,  $\beta$ -DG), the sarcoglycans ( $\alpha$ -,  $\beta$ -,  $\gamma$ -,  $\delta$ -SG), and sarcospan (SSPN) (for review, see Crosbie et al., 1997; Straub and Campbell, 1997). Mutations in the dystrophin gene lead to a high incidence of cardiomyopathy

in Duchenne and Becker muscular dystrophy patients (DMD/BMD) and can cause X-linked dilated cardiomyopathy (Towbin, 1998). Mutations in the genes for the sarcoglycans, a subcomplex of transmembrane proteins within the DGC, are responsible for limb girdle muscular dystrophy (LGMD) (Lim and Campbell, 1998) and can be associated with cardiomyopathy (Melacini et al., 1999). Although various studies of patients with LGMD have shown cardiac involvement, a correlation between the primary mutation and the clinical phenotype of cardiomyopathy has not been established. In addition to these primary genetic causes of cardiomyopathy, recent data suggest that disruption of the DGC underlies the cardiomyopathy associated with enteroviral infection (Badorff et al., 1999). Consequently, evidence is accumulating that the DGC plays a critical role in the pathogenesis of some forms of inherited and acquired cardiomyopathy.

The DGC confers a structural link between laminin-2 in the extracellular matrix and the F-actin cytoskeleton (Ervasti and Campbell, 1993) and is thought to protect muscle cells from contraction-induced damage (Petrof et al., 1993). The tetrameric unit of  $\alpha$ -,  $\beta$ -,  $\gamma$ -, and  $\delta$ -sarcoglycan is a group of single pass transmembrane glycoproteins. Interestingly,  $\alpha$ - and  $\gamma$ -sarcoglycan expression is restricted to skeletal and cardiac muscle tissue (Roberds et al., 1994; Noguchi et al., 1995). In contrast,  $\beta$ -,  $\delta$ -, and  $\epsilon$ -sarcoglycan (an  $\alpha$ -sarcoglycan homolog), along with sarcospan, are additionally expressed in smooth muscle cells (Straub et al., 1999). In order to test the hypothesis that the diversity in tissue expression may be responsible for different pathogenetic mechanisms and distinct clinical phenotypes, we engineered *Sgcd* null mice deficient for  $\delta$ -sarcoglycan (expressed in skeletal, cardiac, and smooth muscle) and compared them to *Sgca* null mice deficient for  $\alpha$ -sarcoglycan (only expressed in skeletal and cardiac muscle).

*Sgca* null mice have recently been reported to display a progressive muscular dystrophy (Duclos et al., 1998). The primary absence of  $\alpha$ -sarcoglycan was accompanied by the concomitant loss of  $\beta$ -,  $\gamma$ -, and  $\delta$ -sarcoglycan and sarcospan in skeletal and cardiac muscle fibers, a phenomenon that is also observed in human forms of sarcoglycanopathies (Lim and Campbell, 1998). Interestingly, although the sarcoglycan–sarcospan (SG-SSPN) complex was absent from the cardiac muscle membrane, no morphological signs of cardiomyopathy were observed (Duclos et al., 1998). In contrast, *Sgcd* null mice exhibited a remarkably different phenotype. These mice displayed a severe muscular dystrophy with large areas of necrosis as a predominant characteristic feature similar to alterations observed in tissue infarcts. In addition, a severe cardiomyopathy developed after the age of 3 months. The predominant pathological features were focal multicellular myocytolytic lesions sharply demarcated from surrounding normal-appearing myocytes. Another striking difference between *Sgca* and *Sgcd* null mice was the disruption of the SG-SSPN complex in vascular smooth muscle (e.g., coronary arteries) of *Sgcd* null mice and preservation of this complex in

<sup>6</sup>To whom correspondence should be addressed (e-mail: kevin-campbell@uiowa.edu).

<sup>7</sup>Both authors contributed equally to this work.

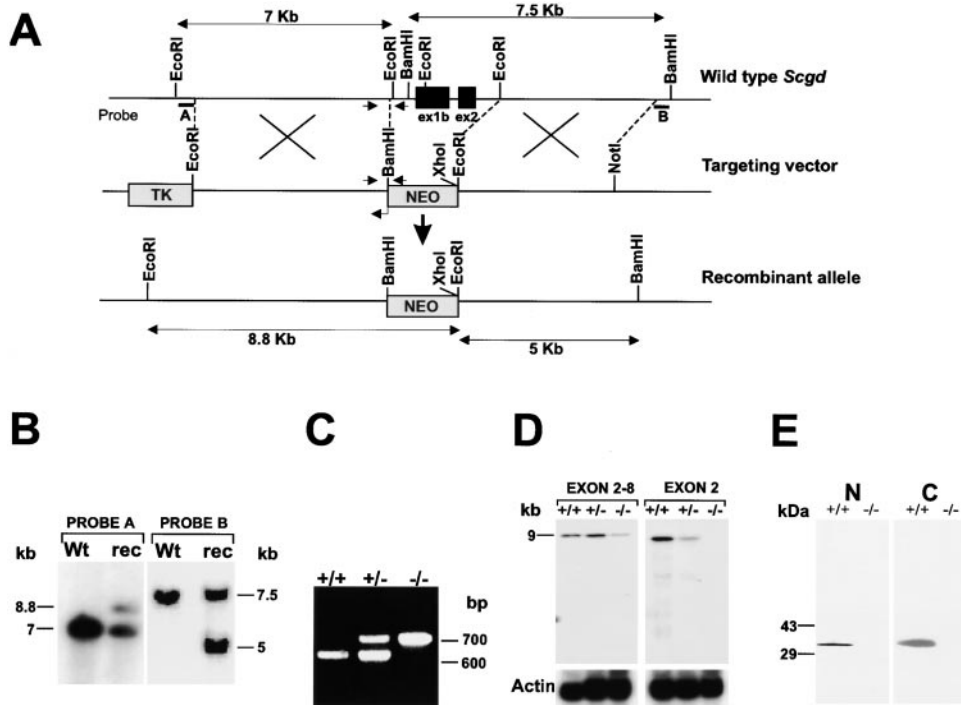


Figure 1. Targeted Disruption of the Mouse *Sgcd* Gene

(A) Restriction map of the 5' portion of the *Sgcd* gene, showing wild-type allele (top), targeting vector (middle), and the predicted targeted allele following homologous recombination (bottom). The position of the *neo* and *tk* cassettes, probes A and B, for Southern analyses, and the primers used for PCR-based genotyping (→) are indicated.

(B) DNA from ES colonies surviving double selection was restricted by EcoRI or BamHI/XhoI and probed by Southern blot with probes A and B, respectively. The replacement of exon 2 by the *neo* cassette yields a new 8.8 kb fragment, which hybridized with probe A in addition to the 7 kb wild-type fragment. As a consequence of the XhoI site introduced by the *neo* cassette, probe B hybridizes with a 5 kb fragment and the 7.5 kb wild-type allele.

(C) PCR analysis of tail DNA purified from wild-type (+/+), heterozygous (+/-), and *Sgcd* null (-/-) mice. The wild-type and targeted alleles produced PCR products of 600 bp and 700 bp, respectively.

(D) Northern analysis of RNA extracted from muscle of wild-type (+/+), heterozygous (+/-), and *Sgcd* null (-/-) mice. A cDNA probe for the complete *Sgcd* gene coding sequence detected a 9 kb transcript in mice of all three genotypes. In contrast, hybridization with a probe corresponding to exon 2 showed the 9 kb transcript only in wild-type (+/+) and heterozygous (+/-) mice.

(E) Immunoblot analysis of skeletal muscle membrane-enriched preparations using an affinity-purified polyclonal antibody against the N-terminal (N) and C-terminal (C) peptide of  $\delta$ -sarcoglycan reveals protein expression in wild-type (+/+) but not *Sgcd* null (-/-) mice.

the *Sgca* null mice. In vivo perfusion of coronary arteries revealed vascular constrictions often associated with pre- and poststenotic dilation and an overall decrease in vessel lumen size in *Sgcd* null mice. These abnormalities preceded the onset of necrosis and were most pronounced at the time of ongoing necrosis. Treadmill exercise-induced stress triggered the onset of multiple focal myocardial lesions in *Sgcd* null mice. Administration of Nicorandil, a vascular smooth muscle relaxant, prevented the development of acute myocardial necrosis in *Sgcd* null mice. These findings suggest a novel pathogenic mechanism whereby disruption of the SG-SSPN complex in vascular smooth muscle causes functional disturbance of the vasculature, which in turn leads to the development of a severe cardiomyopathy and exacerbation of muscular dystrophy in *Sgcd* null mice.

## Results

### Generation of the *Sgcd* Null Mice

In order to create *Sgcd* null mice, a targeting vector was designed to replace exon 2, which encodes 63 amino

acids of the intracellular domain and the entire transmembrane domain (Figure 1A). Southern blot analysis of 370 neomycin-resistant embryonic stem (ES) colonies revealed homologous recombination in seven independent clones (Figure 1B). Two of these heterozygous clones were then used to produce chimeric founder mice. Heterozygous mice from the F1 generation were crossed to obtain *Sgcd* null mice, and the offspring were tested for exon 2 deletion by Southern blot and PCR analysis (Figure 1C). The number of homozygous mutant offspring obtained was the expected 25%, based on Mendelian inheritance. Northern blot analysis, using the complete cDNA coding sequence of  $\delta$ -sarcoglycan gene as a probe, revealed a transcript of 9 kb in the skeletal muscle of wild-type, heterozygous, and homozygous *Sgcd* null mice (Figure 1D). An additional hybridization with a probe specific for exon 2 showed the 9 kb transcript only in the wild-type and heterozygous mice, not in the mutants (Figure 1D). RT-PCR analysis performed with a forward primer in exon 1 and a reverse primer in exon 5 revealed a PCR product representing the normal transcript (600 bp) in wild-type and heterozygous mice

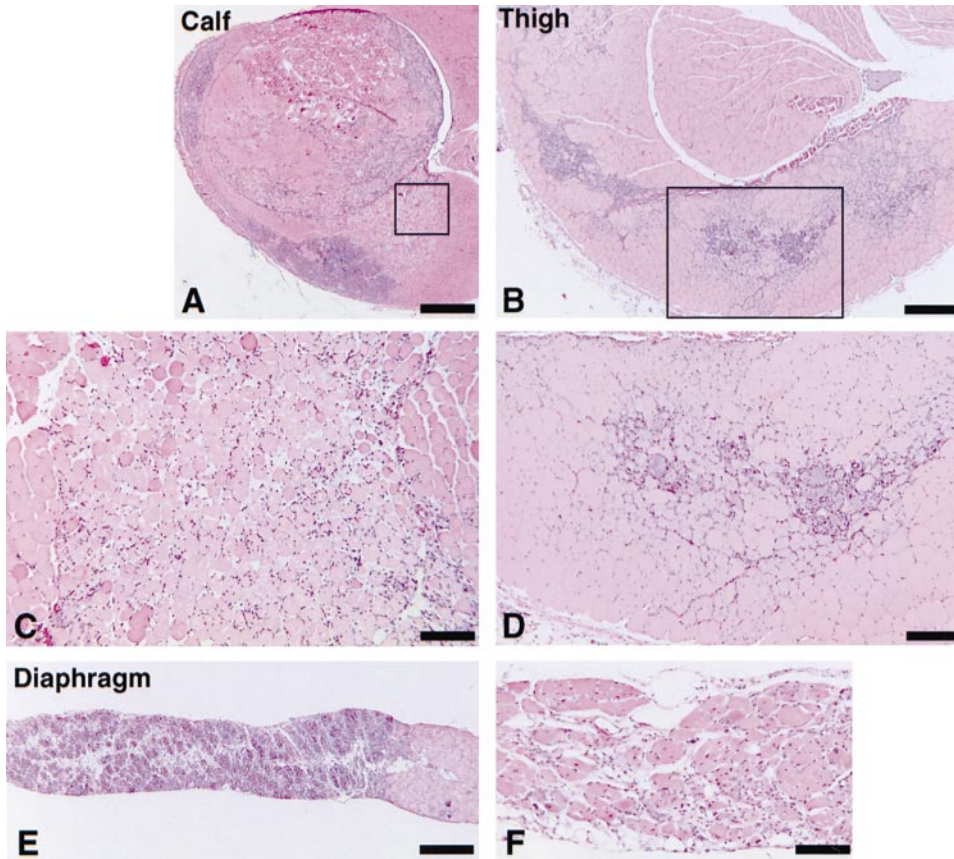


Figure 2. Histological Analysis of *Sgcd*-Deficient Thigh, Calf, and Diaphragm Muscles

Severe dystrophic changes were evident in skeletal muscle at all three sites from a very early age. Shown are calf (A and C), thigh (B and D), and diaphragm (E) from a 1-month-old *Sgcd* null mouse. All but the upper right and lower right corners of the calf muscle in (A) are at various stages of acute necrosis or regeneration. The pale central area of (C) is a higher magnification of an area of acute necrosis similar to that outlined by the black box in (A). Similarly, large areas of necrosis and regeneration in the thigh are shown in (B); the regenerating area within the black box is shown at a higher magnification in (D), where a large percentage of myocytes contain centrally placed nuclei. Regions of full thickness necrosis or regeneration were seen in the diaphragms of these mice (see the purple region on the left of [E]). Chronic dystrophic changes accumulated with age in all of these same muscle groups. Central nucleation, endomysial fibrosis, atrophy, hypertrophy, and fatty infiltration are shown in the diaphragm from a 1-month-old mouse (F). All sections were stained with hematoxylin and eosin. Scale bars represent 1 mm (A), 400  $\mu\text{m}$  (B), 150  $\mu\text{m}$  (C and D), 350  $\mu\text{m}$  (E), and 100  $\mu\text{m}$  (F), respectively.

and an additional PCR product (400 bp) in heterozygous and mutant mice (data not shown). Sequencing of this PCR product suggested that alternative splicing occurred between exon 1 and exon 3 of the  $\delta$ -sarcoglycan gene. In this case, an open reading frame from exon 3 to exon 8 would be maintained. Translation of this smaller transcript would produce a 218 aa protein lacking the entire transmembrane domain and part of the N terminus. However, no protein was detected in the skeletal and cardiac muscle fibers of the *Sgcd* null mice by Western blot of total homogenates and KCl-washed microsomes by using antibodies directed against the C-terminal or N-terminal portion of  $\delta$ -sarcoglycan (Figure 1E). Immunohistochemical analysis of skeletal (data not shown) and cardiac muscle revealed complete absence of  $\delta$ -sarcoglycan with the concomitant loss of the SG-SSPN complex (Figure 5). Overall, the *Sgcd* null mice are fertile, and females can bear at least two litters. Although a controlled aging study is in progress, preliminary data indicate an increased number of spontaneous deaths in *Sgcd* null mice at around 6 months of age.

#### *Sgcd* Null Mice Exhibit a Severe Muscular Dystrophy

In order to examine the effect of targeted disruption of the  $\delta$ -sarcoglycan gene on skeletal muscle morphology, hematoxylin and eosin (H&E)-stained sections of the calf, thigh, and diaphragm muscles were evaluated in wild-type ( $n = 8$ ), *Sgca* and *Sgcd* heterozygous ( $n = 26$ ), and *Sgcd* null mice ( $n = 26$ ) between the ages of 2 weeks and 6 months. *Sgcd* heterozygous mice did not show any morphological abnormalities. Interestingly, the skeletal muscle of the *Sgcd* null mice, even in the very young animals ( $n = 8$ ), showed extensive pathological alterations. The predominant feature was consistent with various stages of skeletal muscle necrosis or regeneration similar to pathological alterations observed in tissue infarcts (Figures 2A–2D). Large regions of necrosis/regeneration were observed in calf and thigh muscles of mice at all ages. Severe necrotic lesions in the diaphragm were predominantly seen in younger animals at 1 month of age (Figures 2E and 2F). Similar findings were observed in a second founder from another cell

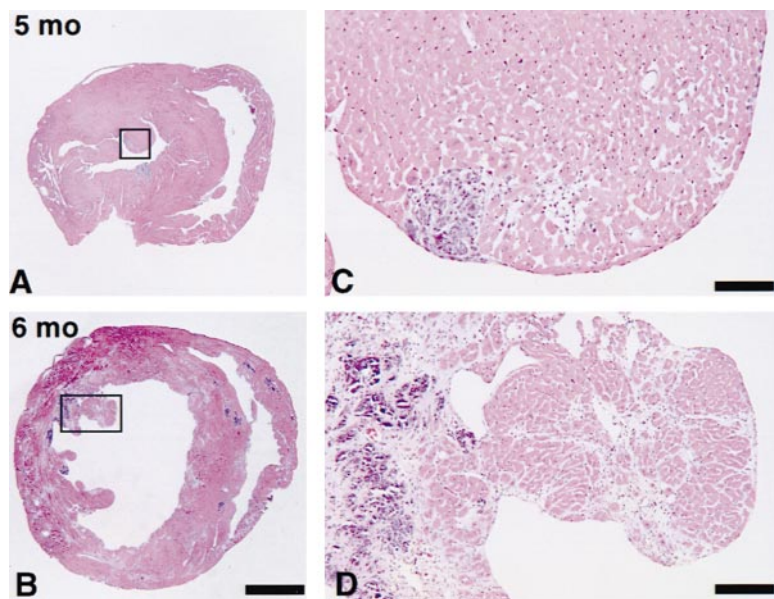


Figure 3. Histological Analysis of *Sgcd*-Deficient Hearts

At the age of 5 months, numerous well-circumscribed regions of myocardial necrosis were observed; two such lesions are present in (A), one in the papillary muscle within the black box and one in the interventricular septum immediately across the ventricle from the black box. A higher magnification of the papillary muscle lesion is shown in (C). By 6 months of age, much more severe cardiomyopathy was present (B). Pathologic changes now included fibrosis (scarring) and calcification in addition to ongoing myocardial necrosis. These changes are more readily discernable in the higher magnification of the papillary muscle (D) that is outlined by the black box in (B). All sections were stained with hematoxylin and eosin. Scale bars represent 1.5 mm (A and B), 75  $\mu$ m (C), and 150  $\mu$ m (D), respectively.

line of targeted ES cells. Based on the evaluation of 200–1100 myofibers per muscle, 80%–100% of nonregenerating myocytes contained internally placed nuclei by the age of 1 month ( $n = 4$ ). In addition to the described severe necrotic/regenerative lesions, a broad spectrum of other dystrophic changes was observed in older (>4 months) *Sgcd*-deficient muscle ( $n = 18$ ). These changes included endomyosial fibrosis, fiber splitting, hypertrophy, dystrophic calcification, and fatty infiltration. Evaluation of creatine kinase (CK) levels in *Sgcd* null mice revealed a 15- to 20-fold elevation of CK as compared to wild-type mice.

#### *Sgcd* Null Mice Display Severe Cardiomyopathy

In order to evaluate whether disruption of the  $\delta$ -sarcoglycan gene may cause cardiac abnormalities, we performed H&E staining of transverse sections of hearts from wild-type ( $n = 8$ ) and *Sgcd* null mice between the ages of 2 weeks and 6 months ( $n = 26$ ). From 2 weeks to 3 months of age ( $n = 8$ ), hearts from *Sgcd* null mice were nearly normal, and only rare, small foci of necrosis were seen. Myocardial tissue studied after 3 months of age revealed more extensive alterations ( $n = 18$ ). Larger and more numerous foci of active cellular necrosis and granular calcium deposits involving small groups of myocytes were present (Figures 3A and 3C). These foci were sharply demarcated from surrounding tissue, which appeared to be normal. The localization and extent of pathology predilection sites varied considerably from animal to animal. In some hearts, subendocardial regions were predominantly affected (Figure 3A), whereas in others, pathological changes in the outer two-thirds of the free walls of both ventricles were observed (Figure 3B). In older animals (5–6 months;  $n = 14$ ), active myocardial necrosis was less evident, but various stages of calcification and fibrosis were observed (Figures 3B and 3D). Interestingly, female mice that had been pregnant at least once ( $n = 4$ ) displayed more widespread and advanced cardiac alterations than age-matched virgin females ( $n = 4$ ). In contrast, extensive histopathological

evaluations of the myocardium of *Sgca* null mice (including pregnant females) showed no pathological alterations besides minimal calcification in some of the older animals (data not shown). No coronary vessel histopathology at the light microscopy level was observed.

In order to evaluate the impact of the morphological changes on electrophysiological function, we performed ECG telemetry in wild-type ( $n = 10$ ), *Sgca* null ( $n = 6$ ), and *Sgcd* null ( $n = 6$ ) mice (Figure 4). Resting heart rates were similar among the three different genotypes, as were PR intervals (a measure of AV nodal conduction). No ventricular arrhythmias were seen in any of the mice. Electrocardiographic characteristics were similar between wild-type and *Sgca* null mice. Ventricular excitation (QRS amplitude and duration), however, was markedly perturbed in the *Sgcd* null mice as compared with wild-type and *Sgca* null mice. The most striking difference between the *Sgcd* null, wild-type, and *Sgca* null mice was the dramatically smaller QRS amplitudes ( $n = 3$ ) consistent with dispersion of depolarization through the ventricle. Consistent with the idea that the fibrotic lesions detected in *Sgcd* null mice underlie the abnormal activation, *Sgcd* null mice ( $n = 3$ ) with less severe pathological findings did not reveal significant ECG abnormalities.

#### Disruption of the SG-SSPN Complex in the Smooth Muscle of the Coronary Arteries in *Sgcd* Null Mice

The characteristic histopathological abnormalities suggested that alterations in vascular smooth muscle might be responsible for these findings. Recent biochemical studies (Straub et al., 1999) suggest that the composition of SG-SSPN complex in smooth muscle is distinct from that in skeletal and cardiac muscle. Consequently, we performed immunohistochemical analysis of components of the DGC in cardiac muscle fibers and smooth muscle cells of coronary arteries from wild-type, *Sgca*, and *Sgcd* null mice (Figure 5). In wild-type mice,  $\alpha$ -,  $\beta$ -,  $\gamma$ -,  $\delta$ -, and  $\epsilon$ -sarcoglycan, sarcospan, and  $\beta$ -dystroglycan were homogeneously expressed at the cardiac muscle fiber membranes.  $\beta$ -,  $\delta$ -, and  $\epsilon$ -sarcoglycan, sarcospan,

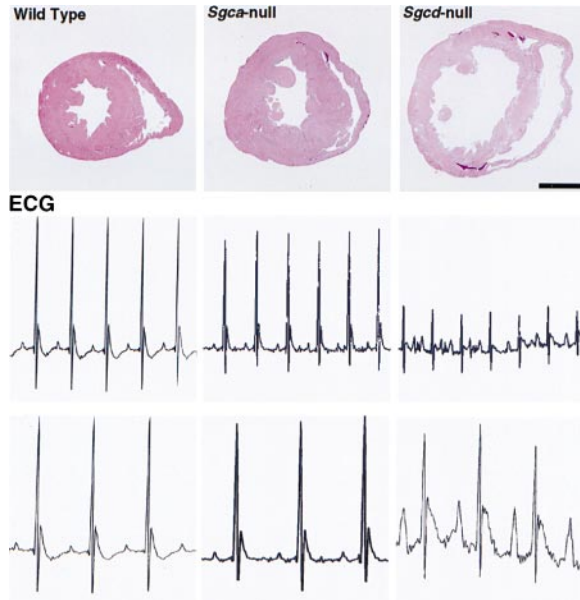


Figure 4. Comparison of Histopathology and ECG Telemetry in Wild-Type, *Sgca*, and *Sgcd* Null Mice

H&E staining of cardiac cross sections of wild-type, *Sgca*, and *Sgcd* null mice reveal cardiomyopathic changes only in *Sgcd* null mice. The *Sgcd*-deficient heart shows severe dilation of the ventricle as well as multiple areas of necrosis and fibrosis. Scale bar represents 1.5 mm. Lead II ECG recordings from conscious mice from three genetic backgrounds (wild-type, *Sgca*, and *Sgcd* null mice) made under identical conditions. In the upper row of ECGs, the horizontal bar corresponds to 100 ms. ECGs in the lower row were enlarged arbitrarily to illustrate QRS morphology.

and  $\beta$ -dystroglycan were also strongly expressed in the smooth muscle cells of the coronary arteries. In contrast,  $\alpha$ - and  $\gamma$ -sarcoglycan were not expressed in smooth muscle cells of coronary arteries. In cardiac muscle fibers of *Sgca* null mice,  $\alpha$ -sarcoglycan was absent from the sarcolemma, whereas  $\delta$ -sarcoglycan was absent from the sarcolemma of *Sgcd* null mice. In addition, there was a concomitant loss of  $\alpha$ -,  $\beta$ -,  $\gamma$ -, and  $\delta$ -sarcoglycan. Sarcospan was absent from the sarcolemma of both animal models. Interestingly,  $\epsilon$ -sarcoglycan was absent from the sarcolemma of *Sgcd* null mice, in contrast to wild-type and *Sgca* null mice. However, the most remarkable difference between the *Sgca* and the *Sgcd* null mice was observed in the expression of the SG-SSPN complex in the smooth muscle of coronary arteries. While  $\beta$ -,  $\delta$ -, and  $\epsilon$ -sarcoglycan, along with sarcospan, were still strongly expressed in the coronary arteries of the *Sgca* null mice, these proteins were completely absent in the smooth muscle cells of *Sgcd* null mice. The same expression pattern was observed in smooth muscle cells of other blood vessels, for example, the femoral artery (data not shown). Western blot analysis of aortic tissue confirmed our immunohistochemical observation that the SG-SSPN complex is disrupted in *Sgcd* null mice, while it is still preserved in aorta from wild-type and *Sgca* null mice (data not shown). Taken together, these results indicate that targeted ablation of the  $\delta$ -sarcoglycan gene leads to disruption of the SG-SSPN complex in smooth muscle, whereas the complex is preserved in smooth muscle cells of *Sgca* null mice.

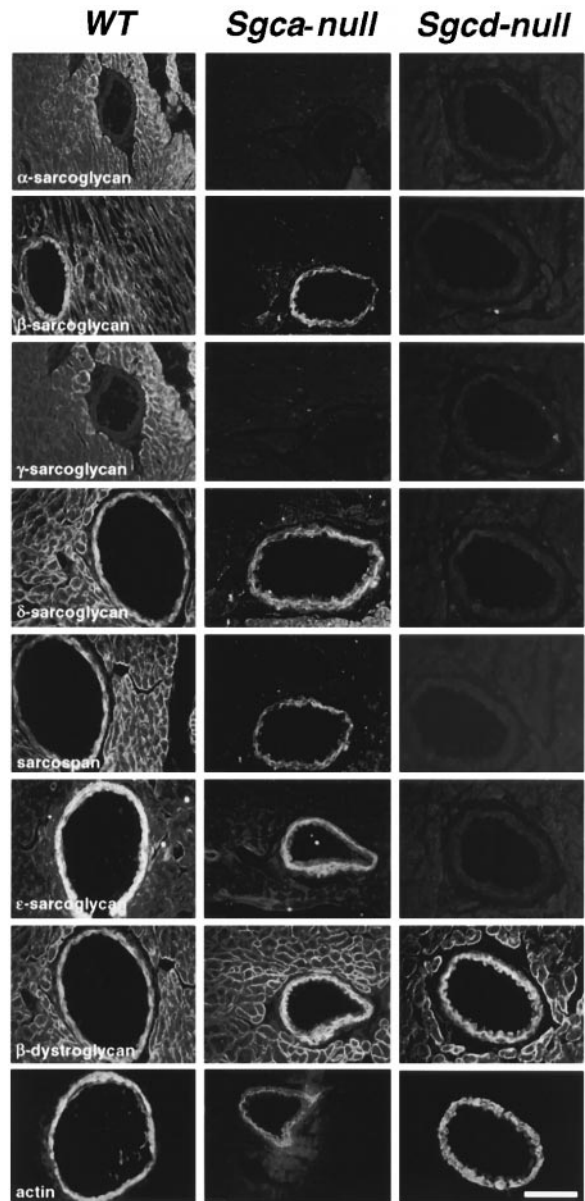


Figure 5. Immunohistochemical Expression of the SG-SSPN Complex in Cardiac Muscle and Smooth Muscle of Coronary Arteries in Wild-Type, *Sgca*, and *Sgcd* Null Mice

In wild-type mice,  $\alpha$ -,  $\beta$ -,  $\gamma$ -,  $\delta$ -, and  $\epsilon$ -sarcoglycan, sarcospan, and  $\beta$ -dystroglycan are strongly expressed in cardiac membranes. In contrast,  $\beta$ -,  $\delta$ -,  $\epsilon$ -sarcoglycan, sarcospan, and  $\beta$ -dystroglycan are expressed in smooth muscle cells of coronary arteries, while  $\alpha$ - and  $\gamma$ -sarcoglycan are not. In *Sgca* and *Sgcd* null mice,  $\alpha$ -,  $\beta$ -,  $\gamma$ -, and  $\delta$ -sarcoglycan, as well as sarcospan, are absent from cardiac membranes, while  $\beta$ -dystroglycan is still present at comparable levels to normal controls. The expression pattern in smooth muscle, though, is strikingly different. In smooth muscle,  $\beta$ -,  $\delta$ -, and  $\epsilon$ -sarcoglycan and sarcospan are absent in coronary arteries of *Sgcd* null mice, while these proteins are still expressed in *Sgca* null mice. Note also the absence of  $\epsilon$ -sarcoglycan at the sarcolemma of *Sgcd* null mice. The expression of  $\beta$ -dystroglycan is not altered in the smooth muscle of *Sgcd* null mice. Staining with an antibody against smooth muscle actin confirmed the presence of smooth muscle in the vasculature. Scale bar represents 20  $\mu$ m.

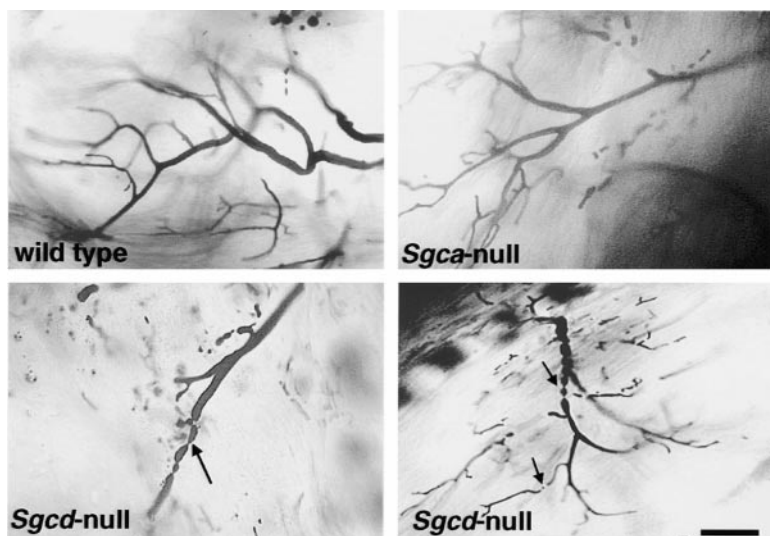


Figure 6. Perfusion of Coronary Artery Vascular Bed

Transillumination of Microfil-perfused coronary arteries in wild-type (upper panel) and *Sgca* null mice (upper right panel) shows smoothly tapered vessels without signs of constriction and/or focal narrowing. In contrast, coronary vessels of *Sgcd* null mice (lower panel) show multiple constrictions (arrows) with pre- and poststenotic dilations as well as narrow vessels with a serrated rather than a smooth contour. Cleared tissue; scale bar represents 40  $\mu$ m.

#### Coronary Artery Vascular Irregularities in *Sgcd* Null Mice

In order to demonstrate whether disruption of the SG-SSPN complex in smooth muscle of coronary arteries indeed leads to vascular perfusion abnormalities, we used the Microfil perfusion technique *in vivo*. We perfused wild-type, *Sgca* null, and *Sgcd* null mice at the age of 2–6 months, and cleared sections of the heart were visualized using transillumination with low-power magnification. The coronary microvessels were distributed normally and were smoothly tapered in both wild-type and *Sgca* null mice (Figure 6). Some animals showed areas of focal vessel narrowing but never showed any severe irregularities. In contrast, *Sgcd* null mice displayed numerous areas of pronounced constrictions. Pre- and poststenotic dilation as an appearance of microaneurysm was frequently associated with these constrictions (Figure 6). Extensive areas of focal vascular lumen narrowing and a generalized sparseness of perfusion were observed. Interestingly, although general perfusion was diminished in capillaries of *Sgcd* null mice, no constrictions were observed. Quantification of vascular abnormalities in *Sgcd* null mice at different ages was determined by calculating the mean numbers of abnormal vessels  $\pm$  SEM in ten nonadjacent microscopic fields at a magnification of 10 $\times$ . No lesions were detected in *Sgca* null and wild-type mice. Analysis of *Sgcd* null mice revealed irregularities in 2- (5  $\pm$  1.1), 4- (11  $\pm$  1.5), and 6-month-old mice (4  $\pm$  0.9) (n = 10 in each age group). However, the most severe and abundant abnormalities were observed at the age of 4 months, a time when acute necrosis was first observed in *Sgcd* null mice. These results indicate that the disturbance of the vasculature precedes the onset of myocardial ischemic lesions.

#### Treadmill Exercise Initiates the Development of Cardiac Muscle Necrosis in Young *Sgcd* Null Mice

In order to test the hypothesis that the observed abnormalities of the vasculature represent a dynamic hyper-reactivity of the vasculature, which may be triggered by stress, we exercised wild-type (n = 20), *Sgca* (n = 20),

and *Sgcd* null mice (n = 42) for 40 min using a treadmill. The exercised mice were studied at the age of 2–3 months, a time where *Sgcd* null mice do not show any overt signs of cardiac muscle necrosis but do have microvessel abnormalities, as revealed by our perfusion studies. All mice were injected with Evans blue dye (EBD) 8 hr before the exercise, and assessment of EBD uptake, as well as routine histopathology, was examined in the cardiac muscle. Interestingly, approximately one-third of the *Sgcd* null mice died suddenly during the exercise, while no death occurred in *Sgca* null and wild-type mice. The surviving *Sgcd* null mice were sacrificed 36–48 hr after exercise for histological assessment of cardiac muscle. All mice displayed multiple areas of EBD uptake corresponding to acute histopathological features of necrosis, as revealed by H&E staining (Figure 7). No signs of necrosis were detected in age-matched, nonexercised *Sgcd* null or wild-type mice. Only a few single necrotic cells were observed in *Sgca* null mice (Figure 7). Quantification of Evans blue staining after treadmill exercise revealed 13%–27% positive stained areas in cardiac muscle sections of *Sgcd* null mice and less than 3% positive stained areas in *Sgca* null mice.

Intraperitoneal administration of Nicorandil, a vascular smooth muscle relaxant, was able to prevent the development of multiple myocardial ischemic lesions in all *Sgcd* null mice (n = 20) studied (Figure 7). Microfil perfusion of coronary arteries in *Sgcd* null mice after administration of Nicorandil revealed no evidence of vascular constrictions and displayed smoothly tapered branches of the coronary vascular bed (Figure 7). Nicorandil, at the dose given, did not lower the systemic blood pressure in *Sgcd* null mice (data not shown). In addition, no alteration of the general behavior during exercise or any cardiac muscle abnormalities were observed during or after exercise of wild-type or *Sgca* null mice after administration of Nicorandil.

#### Discussion

The present study reports that disruption of a sarcoglycan–sarco-span complex in vascular smooth muscle perturbs vascular function, which in turn initiates the development of cardiomyopathy and exacerbates muscular

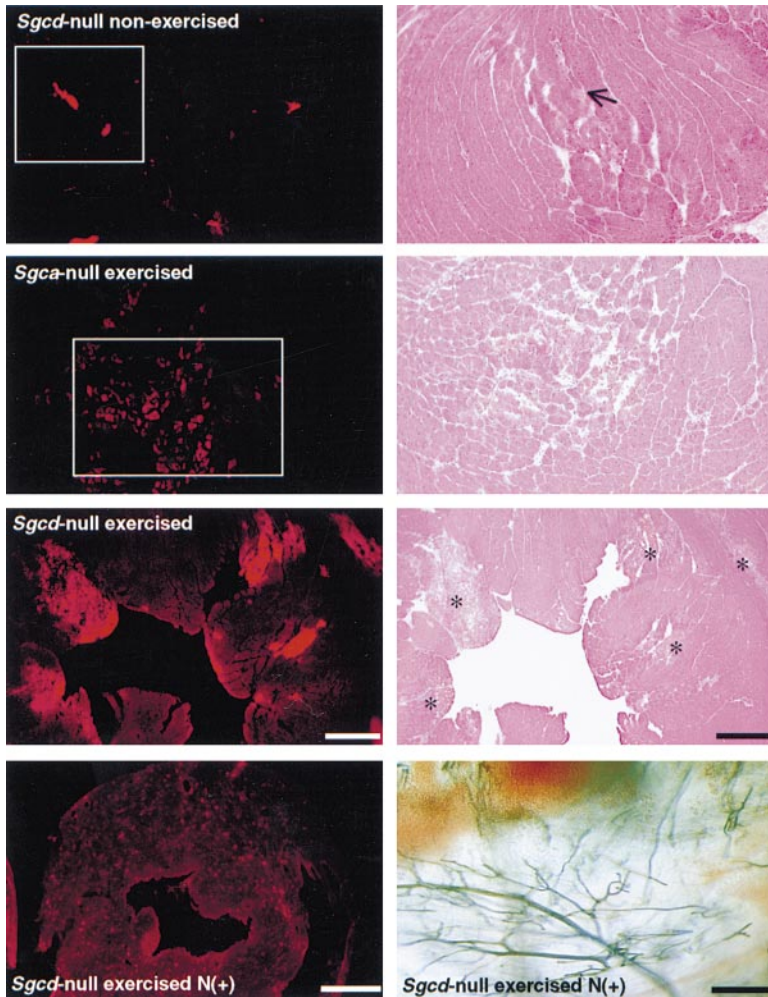


Figure 7. Treadmill Exercise-Induced Myocardial Necrosis Is Prevented by Administration of a Vascular Smooth Muscle Relaxant. Evaluation of Evans blue dye (EBD) uptake and corresponding histopathological assessment reveals no uptake of EBD in nonexercised 2-month-old *Sgcd* null mice (upper panel) and only a few positive EBD cardiomyocytes in *Sgca* null exercised mice corresponding to single cell necrosis (second panel from top). In contrast, *Sgcd* null mice display multiple areas of EBD uptake after treadmill exercise, which correspond to acute histopathological signs of necrosis (second panel from bottom). Each asterisk represents the corresponding area of EBD positive fibers. Scale bar represents 500  $\mu\text{m}$ . No EBD uptake was observed in cardiac muscle of 2-month-old exercised *Sgcd* null mice after intraperitoneal application of Nicorandil for 3 days prior to the exercise (lower left panel). Scale bar represents 1.5 mm. Microfil perfusion of *Sgcd* null mice after Nicorandil treatment displayed no perfusion abnormalities of the vasculature and a smoothly tapered vessel bed (lower right panel). Note also the overall greater density of the vasculature. Scale bar represents 40  $\mu\text{m}$ .

dystrophy in *Sgcd* null mice. Cardiomyopathy is a common clinical phenotype of patients with certain forms of LGMD. Interestingly, cardiac involvement has been described in patients with primary mutations of  $\beta$ -,  $\gamma$ -, and  $\delta$ -sarcoglycan (Nigro et al., 1996; Moreira et al., 1998; Melacini et al., 1999; R. D. C. and T. Voit, unpublished observations), while patients with mutations in the  $\alpha$ -sarcoglycan gene (the most common form of sarcoglycanopathies) only rarely display mild forms of cardiomyopathy (Melacini et al., 1999).

In order to analyze the involvement of sarcoglycans in the pathogenesis of cardiomyopathy and muscular dystrophy, in particular with respect to the different tissue distribution, we analyzed *Sgcd* null mice and compared them with the previously described *Sgca* null mice (Duclos et al., 1998). Morphological evaluation of *Sgca*-deficient hearts revealed no histopathological signs of cardiomyopathy, although the SG-SSPN complex was absent in cardiac muscle membranes. These findings are in accordance with the clinical data observed in patients with primary mutations in the  $\alpha$ -sarcoglycan gene, which also do not display—or display only mildly—cardiomyopathic phenotypes. Interestingly, *Sgcd* null mice developed a severe cardiomyopathy with focal areas of myocardial ischemic-like lesions as the characteristic histopathological feature followed by fibrotic calcification

and scarring of the cardiac muscle. Electrocardiography revealed evidence of dispersion of electrical activation in cardiomyopathic mice in a pattern roughly proportional to the degree of fibrotic change in the left ventricle. This is similar to that seen in patients with cardiomyopathy and indicates that the structural alterations we observed disrupt the wave front of depolarization in the heart.

The essential difference between *Sgca* and *Sgcd* null mice was observed in the expression of the SG-SSPN complex in smooth muscle cells of the vasculature. While in both mutants the expression of the SG-SSPN complex was reduced at the sarcolemma of skeletal and cardiac muscle, the expression of the sarcoglycan-sarcospan complex in smooth muscle cells of the blood vessels was disrupted only in the *Sgcd* null mice. These findings, together with the characteristic ischemic-like lesions in cardiac and skeletal muscle of *Sgcd* null mice, led us to hypothesize that vascular dysfunction may have an essential impact on the development of cardiomyopathy and the severity of muscular dystrophy in *Sgcd* null mice.

In fact, Microfil *in vivo* perfusion of the coronary artery vascular bed of *Sgcd* null mice revealed numerous vessel segments with constrictions and focal luminal narrowing. In contrast, smoothly tapered vessels and a

greater density of small arteries without focal narrowing were detected in wild-type and *Sgca* null mice, both showing normal expression of the SG-SSPN complex in the vascular smooth muscle. The Microfil *in vivo* perfusion enabled us to study long segments of coronary artery branches in three dimensions. Quantification of perfusion abnormalities in *Sgcd* null mice revealed that vessel irregularities are present even in young mice at a stage without any overt signs of cardiac muscle necrosis. Moreover, the most severe and abundant perfusion abnormalities were observed at the time of acute ongoing necrosis, suggesting that a certain degree of vascular dysfunction may be required to reach an ischemic threshold necessary to induce myocardial necrosis. These data indicate that the lesions observed in *Sgcd* null mice are not an induced epiphenomenon caused by alterations of the cardiac muscle *per se*. We propose that increased vascular tone compromises blood supply in a diffuse manner, leading to focal ischemic injury, necrosis, and fibrotic changes.

To confirm the hypothesis that the coronary artery vascular dysfunction initiates the development of myocardial ischemic-like lesions, we first subjected animals to treadmill exercise in order to induce stress and trigger the onset of cardiac muscle necrosis. Treadmill exercise is one of the primary methods used clinically to induce cardiovascular stress in humans and animals (Fewell et al., 1997) and is used to detect cardiovascular abnormalities (e.g., coronary artery dysfunction) that may not be readily apparent at rest. We chose young *Sgcd* null mice at an age before cardiac muscle necrosis developed but when vessel abnormalities were detected. Interestingly, exercise-induced stress initiated the development of multiple focal areas of myocardial ischemic-like lesions in the *Sgcd* null mice. Histological analysis of the myocardial lesions displayed coagulation necrosis, which is a characteristic histological feature observed in conditions associated with myocardial ischemia.

Second, in order to demonstrate that these observations were related to vascular dysfunction, we treated *Sgcd* null mice with Nicorandil, a vascular smooth muscle relaxant compound. Nicorandil has been shown to relax coronary vascular smooth muscle by activation of potassium channels, resulting in hyperpolarization of the smooth muscle membrane, as well as by increasing cyclic GMP levels (Kukovetz et al., 1992). In addition, Nicorandil has been shown to prevent coronary artery vasospasms under a variety of conditions (Kaski, 1995). According to pharmacological studies, dilation of coronary artery microvessels depends on potassium channel activation and is mainly observed at low concentrations of Nicorandil (Kaski, 1995). We therefore applied Nicorandil at a lower dose (1 mg/kg body weight intraperitoneally) to ensure that Nicorandil acted predominantly in the coronary artery microvasculature and did not lower blood pressure. We have been able to successfully prevent mortality and the development of multiple myocardial lesions in treadmill-stressed *Sgcd* null mice. In addition, perfusion studies in Nicorandil-treated *Sgcd* null mice showed the coronary microvascular bed free of constrictions and focal luminal narrowing. We cannot entirely rule out that the disruption of the SG-SSPN complex and the loss of  $\epsilon$ -sarcoglycan in cardiac muscle of

*Sgcd* null mice renders cardiomyocytes more susceptible to the vascular dysfunction. However, we did demonstrate that the functional disturbance of the vasculature initiates ischemic myocardial necrosis. As mice age, this damage develops into a severe cardiomyopathy.

Recently, Hack and colleagues (1998) reported that mice deficient in  $\gamma$ -sarcoglycan develop cardiomyopathy. The authors described primarily fibrotic changes in the ventricular wall. However, there was no report of initial acute necrotic areas in cardiac muscle, and the authors suggested that the cardiomyopathy might be secondary to dystrophic changes of the diaphragm. Another animal model, the BIO 14.6 cardiomyopathic hamster, which has been shown to have a genomic deletion in the  $\delta$ -sarcoglycan gene (Sakamoto et al., 1999), displays cardiac abnormalities similar to the *Sgcd* null mice and associated with microvascular dysfunction (Factor et al., 1982). However, the skeletal muscle of the cardiomyopathic hamster is dystrophic but not as severe as in the *Sgcd* null mice. Although the differences in severity of the skeletal muscle phenotype could be related to physiological differences between mouse and hamster species, another possibility would be that the type of the genetic lesion in each case has distinct influence on the clinical phenotype. In respect to this, it is interesting to note that recent genetic studies revealed expression of  $\delta$ -sarcoglycan transcripts in some tissues of the BIO 14.6 hamster (Sakamoto et al., 1999), suggesting that the BIO 14.6 hamster may not be completely deficient in the  $\delta$ -sarcoglycan protein.

A number of proteins with different subcellular localization in cardiac muscle have been shown to be involved in cardiomyopathy. These proteins include the cytoskeletal proteins actin (Olson et al., 1998) and desmin (Milner et al., 1996), as well as the muscle LIM protein (Arber et al., 1997) and the nuclear lamina protein lamin A/C (Bonne et al., 1999). These studies illustrate that different mechanisms at certain points in cardiac development and in the adult heart involving the cytoskeleton and/or the nuclear lamina of the cardiac muscle can be implicated in the pathogenesis of cardiomyopathy. However, our study opens up an important avenue of research directed toward the involvement of the vascular smooth muscle SG-SSPN complex in the pathogenesis of cardiomyopathy.

We are currently studying the molecular mechanism for the vascular dysfunctions observed in *Sgcd* null mice. Recent biochemical evidence suggests the presence of at least three interconnected subcomplexes—dystrophin, dystroglycan, and sarcoglycan—within the DGC (Crosbie et al., 1999). The results indicate that the expression of each of these subcomplexes is a prerequisite for the structural and functional membrane association of the DGC. It may be possible that the absence of the SG-SSPN complex leads to structural and/or conformational changes of the remaining components of the DGC, which may be related to the abnormal contraction and/or dilation of the vascular smooth muscle. Yet another possibility is that metabolic and signaling pathways are involved in the microvascular dysfunction. Elevated levels of intracellular calcium, disturbances of the nitric oxide synthase pathway, as well as increased activity of protein kinase C, have been implicated in increased contractility and/or spasm of the microvasculature.

In summary, our study provides evidence for a novel mechanism in the pathogenesis of cardiomyopathy and muscular dystrophy. Disruption of the sarcoglycan–sarcospan complex in vascular smooth muscle perturbs vascular function and induces ischemic injury in cardiac and skeletal muscle. This mechanism provides a novel insight into the pathogenesis for these disorders. Thus, future genetic and pharmacological therapeutic approaches will need to be directed not only toward skeletal and cardiac muscle but also toward vascular smooth muscle.

#### Experimental Procedures

##### Isolation of Mouse $\delta$ -SG Genomic and cDNA Clones

One RT-PCR product from mouse skeletal muscle RNA was obtained using the hamster primer HadFor5 (5'-AGCTCAGAGGGGC CACAC-3', exon 2) and the mouse primer MdRev2 (5'-CAGCCAGT GTTCAAGCCAA-3', exon 8). This product, containing exons 2–8 of the  $\delta$ -sarcoglycan gene, was used to screen a Stratagene 129/SV mouse genomic library in vector  $\lambda$ FIXII (La Jolla, CA). Three positive clones were subcloned into pBlueScript KS (+) and restriction enzyme mapped using standard procedures.

##### Generation of *Sgcd* Null Mice

The  $\delta$ -SG targeting vector was constructed using the positive-negative selection vector pPNT. EcoRI and BamHI sites were introduced by high-fidelity PCR mutagenesis (Takara enzyme) at the ends of a 6 kb fragment that contains part of the  $\delta$ -SG intron 1 and exon 1b. The DNA was digested by EcoRI/BamHI and inserted in between the *tk* and *neo* genes of the vector. The second insert was obtained by subcloning a 5 kb NotI–EcoRI  $\delta$ -SG intron 2 fragment into the digested NotI–EcoRI pBlueScript. The insert was isolated by NotI–XhoI digestion and cloned into the NotI and XhoI sites of the plasmid. Following homologous recombination, a portion of intron 1, all of exon 2, and part of intron 2 of the  $\delta$ -SG gene was replaced by the *neo* gene (Figure 1). R1 ES cells were grown and electroporated with 10  $\mu$ g of the NotI-linearized targeting plasmid. Colonies surviving G418 and gancyclovir were isolated, expanded, and screened by Southern blot (Figure 1). ES cell lines from two different correctly targeted clones were injected into C57BL/6J blastocysts and transferred into pseudopregnant females. After germline transmission, DNA was extracted from the offspring's tails, and the genotyping was done by PCR (Figure 1) using the following three different primers in the same reaction: NeoTR (5'-GCTATCAGGACATAGCGTTG GCTA-3'); Mdint1F (5'-GCAAACTTGGAGAGTGAAGAGGC-3'); and Mdint1R (5'-GAGGCATATAAAG TTTGCACGAC-3').

##### Northern Blot Analysis

Total RNA was isolated from wild-type,  $\delta$ -SG (+/–), and  $\delta$ -SG (–/–) skeletal muscle tissue using RNAzol B (Tel-Test) according to the manufacturer's specifications. Twenty micrograms of the RNA was subjected to electrophoresis on a 1.25% agarose gel containing 5% formaldehyde, blotted to Hybond membrane (Amersham), and hybridized with either a 760 bp exon 2–8 probe or an exon 2 probe from mouse  $\delta$ -SG cDNA.

##### Histopathology Studies

Wild-type mice ( $n = 8$ ), *Sgca* and *Sgcd* heterozygous ( $n = 26$ ), and *Sgcd* null mice ( $n = 26$ ) were anesthetized with pentobarbital (0.75 mg/10 g of body weight) via intraperitoneal (IP) injection. Subsequently, the animals were perfused with PBS (15 ml) followed by 15 ml of 10% buffered formalin fixative solution. After embedding the tissue in paraffin, H&E-stained sections (4  $\mu$ m) were prepared in order to characterize skeletal and cardiac muscle pathology. Some animals were sacrificed by cervical dislocation, and H&E staining was performed on cryosections of skeletal and cardiac muscle. Furthermore, H&E sections of brain, lung, liver, kidney, and spleen were performed in some animals. No histopathology was observed in these nonmuscle tissues.

Creatine kinase values were determined in blood serum from wild-type and *Sgcd* null mice using the creatine kinase assay kit from Sigma.

##### Immunofluorescence Analysis

Hearts and skeletal muscle were isolated from wild-type, *Sgca*, and *Sgcd* null mice and rapidly frozen in liquid nitrogen-cooled isopentane. Seven micrometer cryosections were prepared and analyzed by immunofluorescence using different antibodies as described previously (Duclos et al., 1998).

##### Antibodies

Rabbit polyclonal antibodies against  $\alpha$ -sarcoglycan (rabbit 98), dystrophin (rabbit 31), the laminin  $\alpha$ 2 chain,  $\beta$ -sarcoglycan (goat 26),  $\delta$ -sarcoglycan N- and C-terminal peptide (rabbit 214 and 229, respectively), and  $\alpha$ -dystroglycan fusion protein D (goat 20) and against  $\beta$ -dystroglycan C-terminal peptide (rabbit 83), sarcospan, and  $\epsilon$ -sarcoglycan (rabbit 235 and 232, respectively) were described previously (Duclos et al., 1998). An affinity-purified rabbit polyclonal antibody was produced against a COOH-terminal fusion protein (aa 167–291) of  $\gamma$ -sarcoglycan. A commercially available mouse monoclonal antibody was used to detect smooth muscle actin (Sigma).

##### ECG Telemetry

Single-lead ECG recordings were performed in conscious, freely mobile adult mice (3–4 months of age). Surgical anesthesia was achieved with pentobarbital (30–40 mg/kg IP) with occasional exposure to inhaled methoxyflurane. Implantable radio transmitters (Data Sciences International, TA10EA-F20) were implanted in the subcutaneous tissues of the back. Two ECG leads were tunneled under the skin to the ventral aspect of the thorax and sutured to the underlying muscles (ECG lead II configuration). Serial recordings were made on the first three postoperative days.

##### Microfil Perfusion

In order to study coronary microvascular perfusion, mice were anesthetized with phenobarbital (75 mg/kg body weight), and a bilateral sternum incision was performed to expose the left atrium. We perfused 1–1.5 ml of Microfil, a liquid silicon rubber (Flow tech, Carver, MA), into the left atrium. The heart continued beating for about 1 min, and after contraction stopped, the heart was rapidly excised and cured on ice for about 10 min. Adequacy of vascular perfusion was judged by the white blush that developed in the myocardium as well as the white filling of other main arteries (mesenteric artery and femoral artery) of the mouse body. The heart was fixed in 10% formalin for 24 hr, and the next day the tissue was sliced into 2 mm thick transverse cross sections and cleared by sequential 24 hr immersions in 25%, 50%, 75%, 95%, and finally 100% ethyl alcohol. On day 6, specimens were placed in pure methyl salicylate for 12–24 hr. Microvascular perfusion was visualized with both epi- and transillumination and examined under low-power magnification ( $\times 10$ – $20$ ). We quantified the vascular irregularities in *Sgcd* null mice at different ages (2, 4, and 6 months) by counting the number of abnormal individual vessel segments in ten nonadjacent microscopic fields using a low magnification ( $10\times$ ), and the mean number of abnormal vessels was calculated for each mouse. An average number of abnormal vessels  $\pm$  SEM was then calculated for each age group. Vessel segments with more than one abnormality were only counted once.

##### Treadmill Exercise

Animals were exercised using the Omnipacer Treadmill Model LC4/M-MGA/AT (Accuscan Instruments, Inc.), which had an adjustable belt speed (0–100 m/min), shock bars with adjustable amperage, and an on-and-off shock switch for each lane. Animals were exercised at 12–17 m/min for about 10 min and for 25–30 m/min for the remaining 40 min. If an animal became exhausted, the shock bar of this lane was turned off and the animal was allowed to rest at the back of the treadmill for a short period of time. Wild-type ( $n = 20$ ), *Sgca* ( $n = 20$ ), and *Sgcd* null mice ( $n = 42$ ) were divided in approximately equal numbers of males and females. All mice were injected with Evans blue dye (0.5 mg EBD/0.05 ml PBS) intraperitoneally 8 hr before the exercise. Animals were injected with 50  $\mu$ l of this solution per 10 g

body weight. All surviving animals were kept alive for 36–48 hr, and serial sections of cardiac muscle were studied for Evans blue uptake and histopathological signs of necrosis by using routine H&E technique. The effect of Nicorandil treatment on treadmill performance in wild-type ( $n = 6$ ), *Sgca* ( $n = 6$ ), and *Sgcd* null mice ( $n = 20$ ) was studied after 3 days of intraperitoneal injection of Nicorandil at a dose of 1 mg/kg body weight twice a day. Quantification of Evans blue positive stained areas in sections of cardiac muscle from *Sgca* and *Sgcd* null mice ( $n = 20$ , each group) was done by using the Scion image program. The percentage of positive stained areas was calculated by dividing the area of staining by the total area of the analyzed heart section.

#### Acknowledgments

We would like to thank all members of the Campbell laboratory, especially Rachel H. Crosbie, Franck Duclos, Madeleine Durbeej, Michael D. Henry, Jane C. Lee, and David P. Venzke for the critical reading of the manuscript, fruitful discussions, and supply of critical reagents. We want to thank Kathryn Lamping for helpful comments on the pharmacological data. All DNA sequencing was carried out at the University of Iowa DNA Core facility (NIH DK25295). R. D. C. and V. S. were supported by the Deutsche Forschungsgemeinschaft. R. B. was supported by a grant from Telethon Italy N305/b. J. A. H. was supported by a grant from the Roy J. Carver Charitable Trust. R. M. W. was supported by a Grant-in-Aid from the American Heart Association. Histopathology slides were prepared in the Department of Pathology Research Lab. This work was also supported by the Muscular Dystrophy Association (R. W. and K. P. C.). K. P. C. is an Investigator of the Howard Hughes Medical Institute.

Received March 2, 1999; revised July 19, 1999.

#### References

- Arber, S., Hunter, J.J., Ross, J., Jr., Hongo, M., Sansig, G., Borg, J., Perriard, J.C., Chien, K.R., and Caroni, P. (1997). MLP-deficient mice exhibit a disruption of cardiac cytoarchitectural organization, dilated cardiomyopathy, and heart failure. *Cell* **88**, 393–403.
- Badorff, C., Lee G.H., Lamphear, B.J., Martone, M.E., Campbell, K.P., Rhoads, R.E., and Knowlton, K.U. (1999). Enteroviral protease 2 A cleaves dystrophin: evidence of cytoskeletal disruption in an acquired cardiomyopathy. *Nat. Med.* **5**, 320–326.
- Bonne, G., Di Barletta, M.R., Varnous, S., Becane, H.M., Hammouda, E.H., Merlini, L., Muntoni, F., Greenberg, C.R., Gary, F., Urtizberea, J.A., et al. (1999). Mutations in the gene encoding lamin A/C cause autosomal dominant Emery-Dreifuss muscular dystrophy. *Nat. Genet.* **21**, 285–288.
- Crosbie, R.H., Heighway, J., Venzke, D.P., Lee, J.C., and Campbell, K.P. (1997). Sarcospan, the 25-kDa transmembrane component of the dystrophin-glycoprotein complex. *J. Biol. Chem.* **272**, 31221–31224.
- Crosbie, R.H., Lebakken, C.S., Holt, K.H., Venzke, D.P., Straub, V., Lee, J.C., Grady, R.M., Chamberlain, J.S., Sanes, J.R., and Campbell, K.P. (1999). Membrane targeting and stabilization of sarcospan is mediated by the sarcoglycan subcomplex. *J. Cell Biol.* **145**, 153–165.
- Duclos, F., Straub, V., Moore, S.A., Venzke, D.P., Hrstka, R.F., Crosbie, R.H., Durbeej, M., Lebakken, C.S., Ettinger A.J., and van der Meulen, J., et al. (1998). Progressive muscular dystrophy in alpha-sarcoglycan-deficient mice. *J. Cell Biol.* **142**, 1461–1471.
- Ervasti, J.M., and Campbell, K.P. (1993). A role for the dystrophin-glycoprotein complex as a transmembrane linker between laminin and actin. *J. Cell Biol.* **122**, 809–823.
- Factor, S.M., Minase, T., Cho, S., Dorn, R., and Sonnenblick, E.H. (1982). Microvascular spasm in the cardiomyopathic hamster: a preventable cause of focal myocardial necrosis. *Circulation* **66**, 342–354.
- Fewell, J.G., Osinska, H., Klevitsky, R., Willie, N.G., Sfyris, G., Bahreghmand, F., and Robbins, J. (1997). A treadmill exercise regimen for identifying cardiovascular phenotypes in transgenic mice. *Am. J. Physiol.* **273**, H1595–H1605.
- Hack, A.A., Ly, C.T., Jiang, F., Clendenin, C.J., Sigrist, K.S., Wollmann, R.L., and McNally, E.M. (1998). Gamma-sarcoglycan deficiency leads to muscle membrane defects and apoptosis independent of dystrophin. *J. Cell Biol.* **142**, 1279–1287.
- Kaski, J.C. (1995). Management of vasospastic angina—role of Nicorandil. *Cardiovasc. Drugs Ther.* **9**, 221–227.
- Kukovetz, W.R., Holzmann, S., and Poehch, G. (1992). Molecular mechanism of action of Nicorandil. *J. Cardiovasc. Pharmacol.* **20**, S1–S7.
- Lim, L.E., and Campbell, K.P. (1998). The sarcoglycan complex in limb-girdle muscular dystrophy. *Curr. Opin. Neurol.* **11**, 443–452.
- Melacini, P., Fanin, M., Duggan, D.J., Freda, M.P., Berardinelli, A., Danieli, G.A., Barchitta, A., Hoffman, E.P., Dalla Volta, S., and Angelini, C. (1999). Heart involvement in muscular dystrophy due to sarcoglycan gene mutations. *Muscle Nerve* **22**, 473–479.
- Milner, D.J., Weitzer, G., Tran, D., Bradley, A., and Capetanaki, Y. (1996). Disruption of muscle architecture and myocardial degeneration in mice lacking desmin. *J. Cell Biol.* **134**, 1255–1270.
- Moreira, E.S., Vainzof, M., Marie, S.K., Nigro, V., Zatz, M., and Passos-Bueno, M.R. (1998). A first missense mutation in the delta sarcoglycan gene associated with a severe phenotype and frequency of limb-girdle muscular dystrophy type 2F (LGMD2F) in Brazilian sarcoglycanopathies. *J. Med. Genet.* **35**, 951–953.
- Nigro, V., de Sa Moreira, E., Piluso, G., Vainzof, M., Belsito, A., Politano, L., Puca, A.A., Passos-Bueno, M.R., and Zatz, M. (1996). Autosomal recessive limb-girdle muscular dystrophy, LGMD2F, is caused by a mutation in the delta-sarcoglycan gene. *Nat. Genet.* **14**, 195–198.
- Noguchi, S., McNally, E.M., Ben Othmane, K., Hagiwara, Y., Mizuno, Y., Yoshida, M., Yamamoto, H., Bönnemann, C.G., Gussoni, E., Denton, P.H., et al. (1995). Mutations in the dystrophin-associated protein gamma-sarcoglycan in chromosome 13 muscular dystrophy. *Science* **270**, 819–822.
- Olson, T.M., Michels, V.V., Thibodeau, S.N., Tai, Y.S., and Keating, M.T. (1998). Actin mutations in dilated cardiomyopathy, a heritable form of heart failure. *Science* **280**, 750–752.
- Petrof, B.J., Shrager, J.B., Stedman, H.H., Kelly, A.M., and Sweeney, H.L. (1993). Dystrophin protects the sarcolemma from stresses developed during muscle contraction. *Proc. Natl. Acad. Sci. USA* **90**, 3710–3714.
- Roberds, S.L., Leturcq, F., Allamand, V., Piccolo, F., Jeanpierre, M., Anderson, R.D., Lim, L.E., Lee, J.C., Tome, F.M., Romero, N.B., et al. (1994). Missense mutations in the adhalin gene linked to autosomal recessive muscular dystrophy. *Cell* **78**, 625–633.
- Sakamoto, A., Abe, M., and Masaki, T. (1999). Delineation of genomic deletion in cardiomyopathic hamster. *FEBS Lett.* **447**, 124–128.
- Straub, V., and Campbell, K.P. (1997). Muscular dystrophies and the dystrophin-glycoprotein complex. *Curr. Opin. Neurol.* **10**, 168–175.
- Straub, V., Ettinger, A.J., Durbeej, M., Venzke, D.P., Cutshall, S., Sanes, J., and Campbell, K.P. (1999).  $\epsilon$ -sarcoglycan replaces  $\alpha$ -sarcoglycan in smooth muscle to form a unique dystrophin-glycoprotein complex. *J. Biol. Chem.*, in press.
- Towbin, J.A. (1998). The role of cytoskeletal proteins in cardiomyopathies. *Curr. Opin. Cell Biol.* **10**, 131–139.